RESEARCH ARTICLE | MARCH 28 2023

# Piezoelectric substrate-induced strain engineering on tuning polarized Raman spectra of crystalline black phosphorus ⒺⓅ
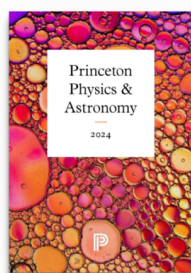
**Special Collection: Energy Conversion and Storage in Functional Dielectrics**

Yuqian Zhao ⓘ ; Feng Guo; Sin-Yi Pang ⓘ ; Weng Fu Io ⓘ ; Lok-Wing Wong ⓘ ; Jiong Zhao ⓘ ;
Jianhua Hao ✉ ⓘ

Check for updates

View Online

Export Citation

02 April 2024 02:08:35

Applied Physics Letters

AIP Publishing

# Piezoelectric substrate-induced strain engineering on tuning polarized Raman spectra of crystalline black phosphorus (EP)

View Online   Export Citation   CrossMark

Yuqian Zhao,[1] (iD) Feng Guo,[1,2] Sin-Yi Pang,[1] (iD) Weng Fu Io,[1] (iD) Lok-Wing Wong,[1] (iD) Jiong Zhao,[1] (iD) and Jianhua Hao[1,2,3,a)] (iD)

### AFFILIATIONS

[1]Department of Applied Physics, The Hong Kong Polytechnic University, Hong Kong 999077, People's Republic of China
[2]The Hong Kong Polytechnic University Shenzhen Research Institute, Shenzhen 518057, People's Republic of China
[3]Research Institute for Smart Energy, The Hong Kong Polytechnic University, Hung Hom, Kowloon, Hong Kong 999077, People's Republic of China

**Note:** This paper is part of the APL Special Collection on Energy Conversion and Storage in Functional Dielectrics.
a)Author to whom correspondence should be addressed: jh.hao@polyu.edu.hk

## ABSTRACT

A black phosphorus (BP) ultrathin nanosheet has significant research values in broad fields ranging from nano-electronics/photonics to quantum physics. Here, a piezoelectric actuator is utilized to perform biaxial strain engineering for the investigation of anisotropic Raman response of the ultrathin BP transferred to the oxide dielectric substrate. Three characteristic peaks exhibit redshift when tensile strain is applied, while the peaks reveal blueshift under compressive strain. When applying compressive strain of $-0.2\%$, the Raman shift rate of $B_{2g}$ mode can reach up to $15.3\,cm^{-1}/\%$. In contrast, with the application of $0.2\%$ tensile strain, the $B_{2g}$ mode is shifted by $-12.2\,cm^{-1}/\%$. Furthermore, we calculated the Grüneisen parameters to deduce the relationship between the tensile or compressive strain and phonon behavior of crystalline BP. The physical mechanism behind the observation of strained Raman response is discussed, which is related to the variations of bond angle and bond length in BP. Additionally, biaxial strain modulation may change the anisotropic dispersion of BP, revealing the significant potential of BP in innovative polarized light detection.

*Published under an exclusive license by AIP Publishing.* https://doi.org/10.1063/5.0143759

Two-dimensional (2D) materials and their wide-ranging applications have generated remarkable research interest.[1–3] Among all, considerable efforts have been placed on dynamic tuning of material interlayer structures to fulfill the requirements of technological innovation.[4,5] Strain engineering has been considered as a powerful tool to carry out the fundamental study of 2D materials and enhance the functionality of devices.[6] In comparison to bulk states, 2D materials with atomic thickness are optimal for the fabrication of flexible optoelectronics as they are dynamically sensitive to external strain and exhibit remarkable flexibility.[7,8] Additionally, strain engineering offers a great path for examining and modifying the electrical and optical transport characteristics because of the quantum confinement and van der Waals (vdW) interaction of the optoelectronic 2D materials along in-plane and out-of-plane directions, respectively.[9,10] So far, both theoretical predictions and practical results have suggested that

the application of strain frequently results in unexpected consequences on 2D layered materials due to the modulation of their lattice structure.[11,12]

There are two typical ways for applying strain on 2D materials. The first method is stretching or bending a 2D material deposited on a flexible substrate to result in uniaxial strain along a specific direction.[13,14] Another approach is utilizing a piezoelectric substrate and generating a biaxial strain.[15,16] In comparison to mechanically induced uniaxial strain, application of biaxial stain is normally regulated by the voltage supplied to the substrate, resulting in more accurate modulation.[17,18] As a result of its outstanding electromechanical and converse piezoelectric capabilities, the single crystalline $(1-x)[Pb(Mg_{1/3}Nb_{2/3})O_3]-x[PbTiO_3]$ (PMN-PT) with $x = 0.3$ was employed as the piezoelectric substrate and strain generated by PMN-PT(001) in this work.[19,20] PMN-PT is recognized as a unique dielectric material that exhibits a substantially high piezoelectric coefficient ($d_{33}$) and electromechanical coupling factor. The $d_{33}$ of

single-crystal bulk PMN-PT ($d_{33} > 2000$ pC/N) is about four times larger than that of Pb[Zr$_x$Ti$_{1-x}$]O$_3$ (PZT) and nearly 30 times more than that of BaTiO$_3$ (BTO).[21]

Black phosphorus (BP) is a layered material with a puckered hexagonal lattice structure, which exhibits a thickness-dependent direct bandgap ranging from around 0.3 (bulk) to 2.3 eV (monolayer) and ultrahigh carrier mobility (more than $1000$ cm$^2$ V$^{-1}$ s$^{-1}$).[22,23] Under the modulation of an external electric field, the bandgap value of BP can be tuned to smaller than 50 meV.[24] The highly tunable BP bandgap can also be affected by adsorption doping and external pressure, which makes BP a viable material for infrared optics.[25,26] Owing to its high in-plane anisotropy, BP can be considered as a building block for novel optoelectronic application with anisotropic characteristics.[27,28] In this work, we evaluate the polarized Raman spectra of mechanically exfoliated layered BP nanosheets under biaxial strain induced by the PMN-PT substrate, demonstrating an efficient technique for modulation and investigation of 2D material characteristics by utilizing an *in situ* and dynamical strategy.

Multilayer BP nanoflakes were mechanically exfoliated onto SiO$_2$/Si substrates from bulk crystals, which were purchased from HQ graphene. Before the transfer process, 30 nm Au thin films were pre-deposited onto the front and back side of the PMN-PT substrate as bottom and top electrodes through electron-beam evaporation, respectively. Since the resistance of gold metal (around 0.02 $\mu\Omega$) is negligible in comparison to the insulating PMN-PT dielectric substrate (G$\Omega$ level), we assume that the bias voltage was mainly dropped to the substrate. Few-layer BP was then dry transferred onto the PMN-PT substrate with polyvinyl alcohol (PVA) film. The temperature was held at 55 °C during the dry transfer process to reduce the interaction between the BP flakes and the substrate. The sample was then covered with PMMA, preventing the degradation of BP in ambient condition. A Keithley 2410 Source Meter was used to supply the bias voltage to the PMN-PT substrate, while an electric field of 10 kV/cm was applied for polarization in advance. Earlier research revealed that a compressive strain was induced by a positive or negative bias voltage.[18] However, in-plane compressive strain was created within the PMN-PT substrate by applying a 500 V bias voltage, while the BP nanosheets and PMMA were simultaneously compressed. Since PMMA is an elastic polymer, which would gradually return to its original state and generated the tensile strain to the BP nanoflakes through the restoration process. Therefore, negative and positive bias voltages with a gradient of 0.04% strain per 100 V were used to apply compressive and tensile strains in this study.

The atomic force microscopy (AFM) measurement was carried out by an Asylum MFP-3D Infinity equipment in the tapping mode to determine the thickness of the few-layer BP flake, which is around 8 nm with a smooth and flat surface [Fig. 1(a)]. High-resolution transmission electron microscopy (HRTEM) (JEOL 2100F) analyses were carried out to further explore the microscopic crystal structure of the mechanically exfoliated BP films. The plan-view picture [Fig. 1(b)] presents a highly ordered configuration of BP atoms with no obvious defects. The lattice constant along [100] direction is 0.327 nm, which concurs with the results from the previous work.[29] The selected-area electron diffraction (SAED) pattern in Fig. 1(c) suggests that the BP sample is highly crystalline and exhibits a typical orthogonal lattice.

To investigate the vibrational behavior of BP on PMN-PT substrate under different strain conditions, the schematic diagram of Raman measurements of BP under biaxial strain generated by the piezoelectric substrate is shown in Fig. 2(a). The Raman spectra were studied using a WITEC Confocal Raman system with a 532 nm laser as an excitation source and a spot size of 1 $\mu$m to determine the vibration and optical characteristics. Moreover, a low laser power (less than 0.5 mW) was employed during the experiments to prevent sample damage. As presented in Fig. 2(b), the three characteristic Raman peaks are positioned at 365, 442, and 471 cm$^{-1}$, corresponding to out-of-plane mode (A$_g^1$), in-plane mode along zig–zag direction (B$_{2g}$), and in-plane mode along armchair direction (A$_g^2$), respectively, which is consistent with the previous literature.[30]

Polarized Raman spectra were collected from the same sample to further investigate the electron–photon and electron–phonon interactions of BP. The tests were repeated at same position of the identical sample in 15° increments from 0° to 180° for better variable control and data reliability, which are corresponding to the angle between the polarization direction of the incident laser and the sample orientation. Figure 3(a) illustrates that the direction of initial polarized incident laser is parallel to the analyzer, while the Raman intensities of the three typical modes demonstrate a substantial reliance on the polarization angles. As the A$_g^1$ and A$_g^2$ modes have similar trend and practically vanish at 0° and arrive at their vertices at 90°, the polar plot of A$_g^2$ mode is displayed in Fig. 3(b). In contrast, the B$_{2g}$ mode exhibits the opposite tendency, which has highest intensity at 0° and lowest intensity at 90°. Because of the anisotropic structure of BP, it can be
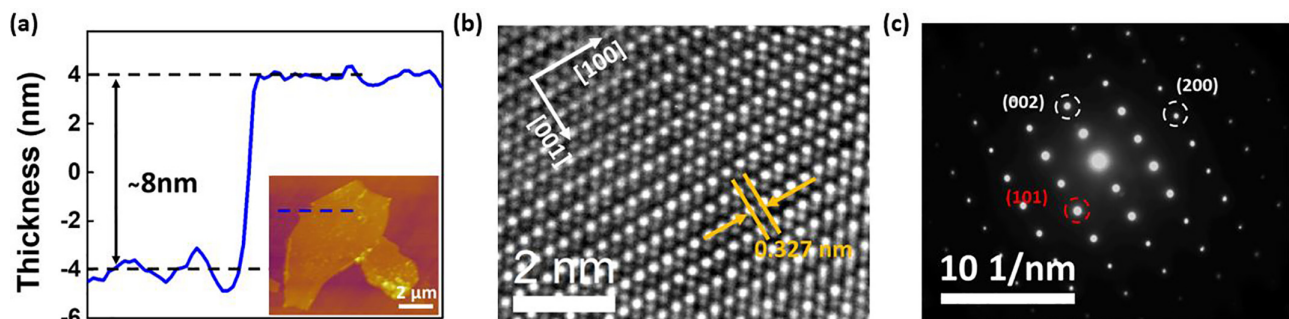
**FIG. 1.** (a) The AFM height profile of BP nanosheet prepared through mechanical exfoliation. Inset: corresponding AFM image. (b) HRTEM and (c) the corresponding SEAD pattern of the BP nanoflake.
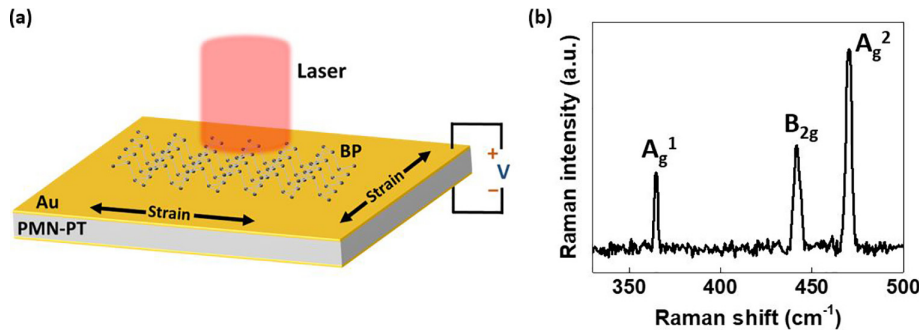
**FIG. 2.** (a) Schematic illustration of Raman spectra acquired with an electro-mechanical device inducing external biaxial strain. (b) Raman spectrum of BP nanoflake under strain-free condition.

identified that the variation of intensities of these three peaks differs from one another.[31]

The typical Raman spectra of a BP nanoflake under various biaxial tensile and compressive strains using a non-polarized configuration can be observed in Fig. 4(a). The redshift of three characteristic peaks can be observed with the application of tensile strain, whereas the peaks exhibit blueshift with compressive strain. For the applied compressive strain of $-0.2\%$, the $A_g^1$, $B_{2g}$, and $A_g^2$ modes shifted by 6.2, 15.3, and $12.2\,\text{cm}^{-1}/\%$, respectively. In contrast, the $A_g^1$, $B_{2g}$, and $A_g^2$ modes shifted by $-6.2$, $-12.2$, and $-12.2\,\text{cm}^{-1}/\%$, respectively, with the application of 0.2% tensile strain. When strain is applied to 2D materials, the change in lattice constant and vibrational behavior is expected to lead to the shift of Raman peak.[32] The out-of-plane $A_g^1$ mode corresponding to the top and bottom phosphorus atoms in the same layer vibrating oppositely to one another. The in-plane vibration of the phosphorus atoms in different orientations is correlated with the $B_{2g}$ and $A_g^2$ modes. Since the PMN-PT substrate was able to generate in-plane biaxial strain, the horizontal crystal deformation of BP was greater than the vertical one, indicating that the $B_{2g}$ and $A_g^2$ modes were more sensitive. The Grüneisen parameter $\gamma$ can be used for describing the rate of phonon frequency fluctuations as a function of strain. $\gamma$ is defined as follows:

$$\gamma = \frac{-1}{2\omega_0}\frac{\partial\omega}{\partial\varepsilon},\qquad(1)$$

where $\omega_0$ and $\omega$ are the Raman frequencies under strain-free and finite biaxial strain conditions, respectively, and $\varepsilon$ is the biaxial strain applied. In our work, it can be simplified as the following formula:

$$\gamma = -\frac{\Delta\omega}{2\omega_0}.\qquad(2)$$

Herein, the Grüneisen parameters for $A_g^1$, $B_{2g}$, and $A_g^2$ modes under $-0.2\%$ compressive strain are $-1.28$, $-1.74$, and $-1.30$, respectively. For 0.2% tensile strain, the Grüneisen parameters are 1.28, 1.39, and 1.30, respectively. The value of $B_{2g}$ Grüneisen parameter under compressive strain is slightly larger than that of tensile strain. This can be ascribed to the slippage during the strain application procedure, and the strain induced by the piezoelectric PMN-PT substrate might not have been entirely transferred onto the BP nanoflakes. Comparing our result to the Grüneisen parameters of $MoS_2$ (around 1.06 under uniaxial strain)[33] and previously reported $A_g^2$ Grüneisen parameter for BP through uniaxial tensile strain (around 0.01 along armchair direction)[34] suggests that piezoelectric substrate-induced biaxial strain can be considered as an additional powerful tool for further modification and investigation of lattice vibration.

Figure 4(b) displays the BP structure with five structural parameters, while $A_1$, $A_2$, and $A_3$ represent the three distances between P atoms, and $\theta_1$ and $\theta_2$ represent the two angles between P atoms. As aforementioned, the $A_g^1$ mode refers to atomic vibration that occurs predominantly along the out-of-plane direction with a small portion
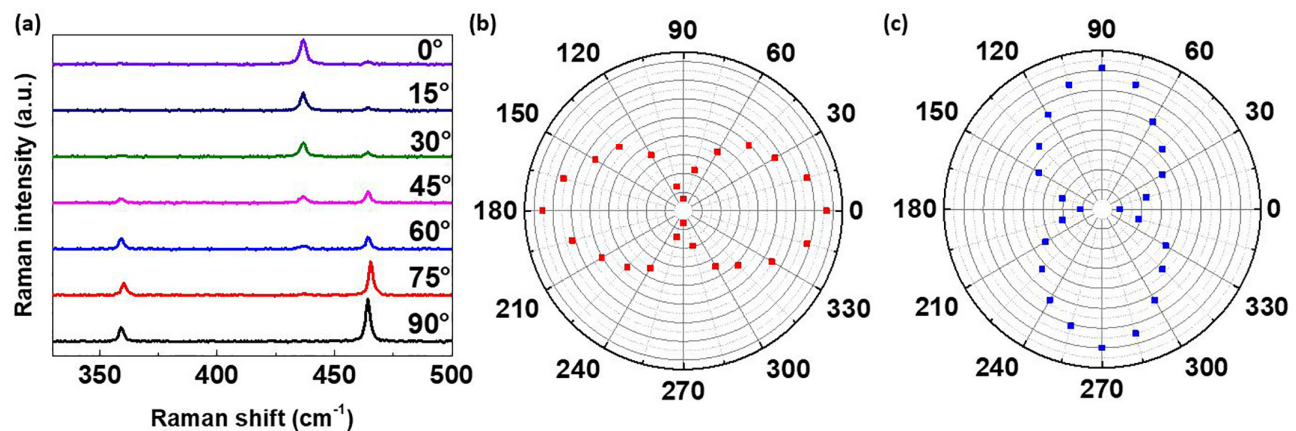


**FIG. 3.** (a) Polarized Raman spectra of BP nanosheets at various polarization angles. Polar plots based on polarized Raman peak intensities of (b) $A_g^2$ and (c) $B_{2g}$ modes.
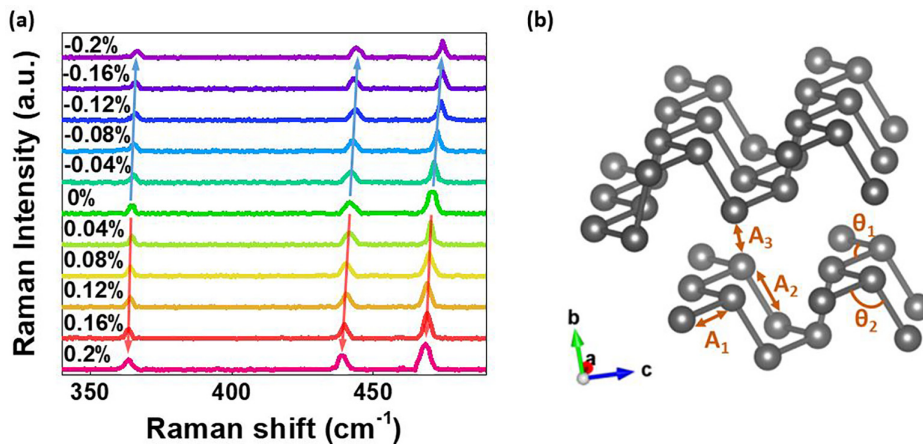
**FIG. 4.** (a) Raman spectra of BP sample on the PMN-PT substrate under different biaxial strains. (b) The 3D model of BP structure with structure parameter definitions.

along the in-plane direction and orthogonal to $A_g^2$ mode. In contrast, $B_{2g}$ mode functions entirely at in-plane orientation, which exhibits different reliance on structural parameters. Altering $A_1$, $A_2$, and $\theta_1$ has little effect on the vibration of the $A_g^1$ mode since it occurs mostly in the out-of-plane direction. Comparatively, changes in $A_3$ and $\theta_2$ are more likely to cause the shift of $A_g^1$. The applied strain significantly enhances or depresses $\theta_2$ shear-like motion between two nearby sublayers. While in-plane restoring force between the two sublayers is increased, the out-of-plane one is reduced, resulting in softening the $A_g^1$ mode and enhancing the $A_g^2$ mode. When the applied tensile strain stretches $A_1$ and enlarge $\theta_1$, the separation of atoms in the sublayer along y axis is extended, reducing the restoring force along x and y axes. This can be considered as the contribution to the significant redshifts of $B_{2g}$ and $A_g^2$ modes. The strength of the interlayer interaction is reflected by the value of $A_3$, which has very little impact on the frequency shifts of optical modes due to its low intensity, indicating that the interlayer restoring forces is negligible when compared to the interlayer ones (in-plane and out-of-plane directions).[35] As a result, the influence of modifying $A_3$ can be excluded.

The Raman spectra at various strain conditions are shown in Fig. 5(a). The intensities of three Raman peaks are increased and decreased with the application of tensile and compressive strain, respectively. Here,

we focus on BP in-plane $B_{2g}$ and $A_g^2$ Raman peaks by considering that the anisotropic optical properties of few-layer BP with biaxial strain are more sensitive than those inside the interlayer structure. Figures 5(b) and 5(c) demonstrate the polar plot of the polarized Raman intensities of $B_{2g}$ and $A_g^2$ peaks under different strains, respectively. It is worth noting that the Raman peak intensity of $A_g^1$ mode is still out of phase with the $B_{2g}$ and $A_g^2$ modes and consistent with the results displayed in Figs. 3(b) and 3(c). After the modulation of 0.2% tensile strain and −0.2% compressive strain, the peak intensity of $B_{2g}$ mode was enhanced by around 35% and reduced by 14% at 90°, respectively, but almost remain the same at 0°. In contrast, the Raman intensities of $A_g^2$ peaks increased by about 29% and decreased by 12% at 0°, respectively, with little change at 90°. The BP crystal exhibits comparable deformation in the armchair and zigzag directions. It can be deduced that $A_g^2$ and $B_{2g}$ modes in the armchair and zigzag directions show stronger electron–phonon interactions under tensile strain and weaker interactions under compressive strain with polarization light at 0° and 90°, respectively.

In conclusion, we have identified that the characteristics of BP polarized Raman spectra are highly tunable with application of biaxial strain induced with the piezoelectric PMN-PT substrate. Biaxial strain can be induced and applied to BP samples by varying bias voltage on the substrate accurately, which results in a noticeable shift in Raman
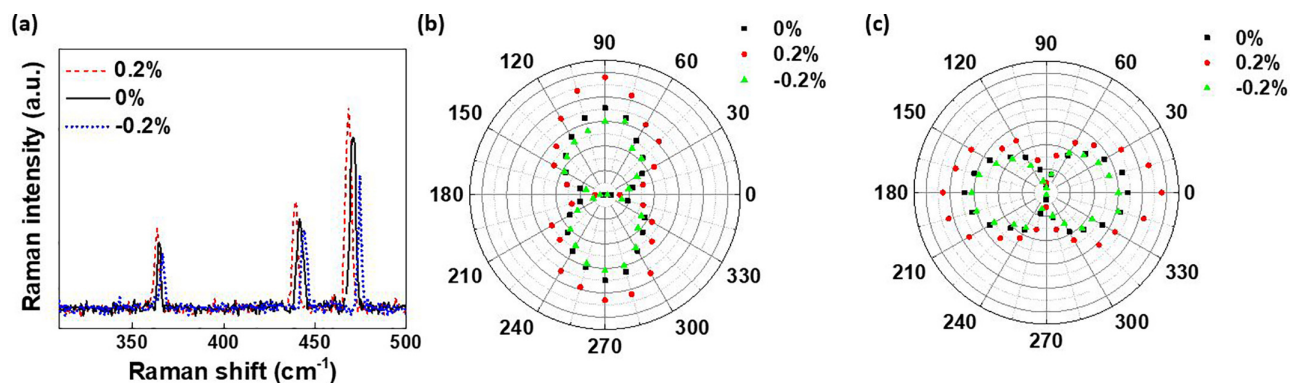


**FIG. 5.** (a) Polarized Raman spectra of the BP nanoflake under strain-free, 0.2% tensile strain, and −0.2% compressive strain conditions. Inset: The magnified graph around $A_g^1$ peak. Corresponding polar plots based on polarized Raman peak intensities of (b) $B_{2g}$ and (c) $A_g^2$ modes under different biaxial strain conditions.

spectra. The Grüneisen parameter is calculated to investigate the vibrational behavior of ultrathin BP under various strain conditions. The strain response in BP may be attributed to changes in the bond lengths and angles as a result of applied biaxial strain. By analyzing the polarized Raman spectroscopy outcomes, we found that the electron–phonon interactions can be modulated by biaxial strain. Our research provides an efficient method for examining the effects of the piezoelectric PMN-PT substrate on the electrical and optical properties of BP materials, which has the potential to be broadened to explore other strain-dependent phenomena and diverse device applications in electronics, photonics, mechanical strain sensing, and energy harvesting fields.

## AUTHOR DECLARATIONS
### Conflict of Interest

The authors have no conflicts to disclose.

### Author Contributions

**Yuqian Zhao:** Conceptualization (equal); Data curation (equal); Investigation (equal); Methodology (equal); Writing – original draft (equal); Writing – review & editing (equal). **Feng Guo:** Conceptualization (equal); Writing – original draft (equal); Writing – review & editing (equal). **Sin-Yi Pang:** Data curation (equal); Visualization (equal). **Weng Fu Io:** Data curation (equal); Methodology (equal); Visualization (equal). **Lok Wing WONG:** Data curation (equal). **Jiong ZHAO:** Data curation (equal). **Jianhua Hao:** Funding acquisition (lead); Supervision (lead); Writing – original draft (lead); Writing – review & editing (lead).

## DATA AVAILABILITY

The data that support the findings of this study are available within the article.

## REFERENCES

[1]Y. Liu, Y. Huang, and X. Duan, Nature **567**, 323 (2019).
[2]S. Yuan, S. Y. Pang, and J. Hao, Appl. Phys. Rev. **7**, 021304 (2020).
[3]S. Y. Pang, W. F. Io, L. W. Wong, J. Zhao, and J. Hao, Nano Energy **103**, 107835 (2022).
[4]W. F. Io, M. C. Wong, S. Y. Pang, Y. Zhao, R. Ding, F. Guo, and J. Hao, Nano Energy **99**, 107371 (2022).
[5]E. M. Mannebach, C. Nyby, F. Ernst, Y. Zhou, J. Tolsma, Y. Li, M. J. Sher, I. C. Tung, H. Zhou, Q. Zhang, and K. L. Seyler, Nano Lett. **17**, 7761 (2017).
[6]T. Dong, J. Simões, and Z. Yang, Adv. Mater. Interfaces **7**, 1901657 (2020).
[7]J. Mao, Z. Wu, F. Guo, and J. Hao, ACS Appl. Mater. Interfaces **14**, 36052 (2022).
[8]S. J. Kim, K. Choi, B. Lee, Y. Kim, and B. H. Hong, Annu. Rev. Mater. Res. **45**, 63 (2015).
[9]S. Yang, Y. Chen, and C. Jiang, InfoMat **3**, 397 (2021).
[10]G. G. Naumis, S. Barraza-Lopez, M. Oliva-Leyva, and H. Terrones, Rep. Prog. Phys. **80**, 96501 (2017).
[11]Y. Qi, M. A. Sadi, D. Hu, M. Zheng, Z. Wu, Y. Jiang, and Y. P. Chen, Adv. Mater. **11**, e2205714 (2022).
[12]Z. Peng, X. Chen, Y. Fan, D. J. Srolovitz, and D. Lei, Light: Sci. Appl. **9**, 190 (2020).
[13]W. Wu, L. Wang, Y. Li, F. Zhang, L. Lin, S. Niu, D. Chenet, X. Zhang, Y. Hao, T. F. Heinz, and J. Hone, Nature **514**, 470 (2014).
[14]Y. Zhao, F. Guo, R. Ding, W. F. Io, S. Y. Pang, W. Wu, and J. Hao, Adv. Opt. Mater. **9**, 2100864 (2021).
[15]F. Ding, H. Ji, Y. Chen, A. Herklotz, K. Dörr, Y. Mei, A. Rastelli, and O. G. Schmidt, Nano Lett. **10**, 3453 (2010).
[16]S. S. Won, H. Seo, M. Kawahara, S. Glinsek, J. Lee, Y. Kim, C. K. Jeong, A. I. Kingon, and S. H. Kim, Nano Energy **55**, 182 (2019).
[17]W. Jie, Y. Yu Hui, Y. Zhang, S. Ping Lau, and J. Hao, Appl. Phys. Lett. **102**, 223112 (2013).
[18]F. Guo, Y. Lyu, M. B. Jedrzejczyk, Y. Zhao, W. F. Io, G. Bai, W. Wu, and J. Hao, Appl. Phys. Lett. **116**, 113101 (2020).
[19]R. Pramanik, M. K. Sahukar, Y. Mohan, B. Praveenkumar, S. R. Sangawar, and A. Arockiarajan, Ceram. Int. **45**, 5731 (2019).
[20]G. T. Hwang, H. Park, J. H. Lee, S. Oh, K. I. Park, M. Byun, H. Park, G. Ahn, C. K. Jeong, K. No, and H. Kwon, Adv. Mater. **26**, 4880 (2014).
[21]S. Xu, Y. Yeh, G. Poirier, M. C. McAlpine, R. A. Register, and N. Yao, Nano Lett. **13**, 2393 (2013).
[22]Z. Wu and J. Hao, npj 2D Mater. Appl. **4**, 4 (2020).
[23]Y. Zhao, Z. Wu, Z. Dang, and J. Hao, Appl. Phys. Rev. **9**, 041318 (2022).
[24]B. Deng, R. Frisenda, C. Li, X. Chen, A. Castellanos-Gomez, and F. Xia, Adv. Opt. Mater. **6**, 1800365 (2018).
[25]H. Hu, Z. Shi, K. Khan, R. Cao, W. Liang, A. K. Tareen, Y. Zhang, W. Huang, Z. Guo, X. Luo, and H. Zhang, J. Mater. Chem. **8**, 5421 (2020).
[26]Z. Xiang, G. Ye, C. Shang, B. Lei, N. Wang, K. Yang, D. Liu, F. Meng, X. Luo, L. Zou, and Z. Sun, Phys. Rev. Lett. **115**, 186403 (2015).
[27]N. Mao, J. Tang, L. Xie, J. Wu, B. Han, J. Lin, S. Deng, W. Ji, H. Xu, K. Liu, and L. Tong, J. Am. Chem. Soc. **138**, 300 (2016).
[28]J. Qiao, X. Kong, Z. X. Hu, F. Yang, and W. Ji, Nat. Commun. **5**(1), 4475 (2014).
[29]Z. Wu, Y. Lyu, Y. Zhang, R. Ding, B. Zheng, Z. Yang, S. P. Lau, X. H. Chen, and J. Hao, Nat. Mater. **20**, 1203 (2021).
[30]H. Liu, A. T. Neal, Z. Zhu, Z. Luo, X. Xu, D. Tománek, and P. D. Ye, ACS Nano **8**, 4033 (2014).
[31]X. Ling, S. Huang, E. H. Hasdeo, L. Liang, W. M. Parkin, Y. Tatsumi, A. R. Nugraha, A. A. Puretzky, P. M. Das, B. G. Sumpter, and D. B. Geohegan, Nano Lett. **16**, 2260 (2016).
[32]Y. Wang, C. Cong, W. Yang, J. Shang, N. Peimyoo, Y. Chen, J. Kang, J. Wang, W. Huang, and T. Yu, Nano Res. **8**, 2562 (2015).
[33]H. Conley, B. Wang, J. Ziegler, R. Haglund, Jr., S. Pantelides, and K. Bolotin, Nano Lett. **13**, 3626 (2013).
[34]Y. Li, Z. Hu, S. Lin, S. K. Lai, W. Ji, and S. P. Lau, Adv. Funct. Mater. **27**, 1600986 (2017).
[35]Z. X. Hu, X. Kong, J. Qiao, B. Normand, and W. Ji, Nanoscale **8**, 2740 (2016).